



# Measurement of $^{15}\text{N}$ longitudinal relaxation rates in $^{15}\text{NH}_4^+$ spin systems to characterise rotational correlation times and chemical exchange



D. Flemming Hansen

*Institute of Structural and Molecular Biology, Division of Biosciences, University College London, London WC1E 6BT, United Kingdom*

## ARTICLE INFO

### Article history:

Received 2 December 2016

Revised 16 January 2017

Accepted 20 January 2017

### Keywords:

$\text{AX}_4$  spin systems

NMR

Nuclear spin relaxation

Ammonium

Chemical exchange

## ABSTRACT

Many chemical and biological processes rely on the movement of monovalent cations and an understanding of such processes can therefore only be achieved by characterising the dynamics of the involved ions. It has recently been shown that  $^{15}\text{N}$ -ammonium can be used as a proxy for potassium to probe potassium binding in bio-molecules such as DNA quadruplexes and enzymes. Moreover, equations have been derived to describe the time-evolution of  $^{15}\text{N}$ -based spin density operator elements of  $^{15}\text{NH}_4^+$  spin systems. Herein NMR pulse sequences are derived to select specific spin density matrix elements of the  $^{15}\text{NH}_4^+$  spin system and to measure their longitudinal relaxation in order to characterise the rotational correlation time of the  $^{15}\text{NH}_4^+$  ion as well as report on chemical exchange events of the  $^{15}\text{NH}_4^+$  ion. Applications to  $^{15}\text{NH}_4^+$  in acidic aqueous solutions are used to cross-validate the developed pulse sequence while measurements of spin-relaxation rates of  $^{15}\text{NH}_4^+$  bound to a 41 kDa domain of the bacterial Hsp70 homologue DnaK are presented to show the general applicability of the derived pulse sequence. The rotational correlation time obtained for  $^{15}\text{N}$ -ammonium bound to DnaK is similar to the correlation time that describes the rotation about the threefold axis of a methyl group. The methodology presented here provides, together with the previous theoretical framework, an important step towards characterising the motional properties of cations in macromolecular systems.

© 2017 The Author. Published by Elsevier Inc. This is an open access article under the CC BY license (<http://creativecommons.org/licenses/by/4.0/>).

## 1. Introduction

Monovalent cations such as potassium and sodium regulate many enzymes via binding to either active sites or to allosteric sites [1–3]. The dynamics and movements of these ions are therefore crucial factors to understand the regulation of enzymes by monovalent cations and experimental insight into the dynamics of cations therefore becomes important in order to characterise many biological processes. Solution NMR spectroscopy is a powerful technique to probe the dynamics of nuclear spin, where in particular nuclear spin-relaxation rates have been used to report on the dynamics of small ions [4–7] to large macromolecular complexes [8–11]. The obtained nuclear spin-relaxation rates often report on both the rotational correlation time of the nuclear spin as well as on chemical exchange between different magnetic environments and a separation of the different contributions to the observed nuclear spin-relaxation rate is thus important. Several strategies have therefore previously been employed to separate the different contributions to spin-relaxation rates, including, measurements at several magnetic field strengths [12], measurements

of cross-correlated relaxation rates [13,14], and measurements of the relaxation rate of related anti-phase coherences [15,16].

Recently it was shown that  $^{15}\text{NH}_4^+$  can be used as a proxy for potassium to probe potassium-binding sites in nucleic acids and enzymes [17–20]. This method relies on several characteristics of the ammonium ion: (i) The ionic radius of the ammonium ion is similar to the ionic radius of potassium, 1.44 Å versus 1.33 Å [21,22], such that ammonium generally binds to potassium binding-sites in macromolecules. (ii) Under physiological conditions the chemical exchange of the ammonium protons with the bulk solvent is so fast that free ammonium is not observed in NMR correlation spectra, however, the protection of the ammonium ion, for example by a protein environment, slows the exchange of the protons with the bulk solvent to such an extent that these are observed in two-dimensional  $^{15}\text{N}$ - $^1\text{H}$  correlation spectra [19]. (iii) Finally, protein-bound ammonium ions appear to have a fast internal correlation time such that the line broadening due to the  $^{15}\text{N}$ - $^1\text{H}$  dipolar-dipole interactions is limited.

The recently developed theory for  $^{15}\text{N}$  spin relaxation in  $^{15}\text{NH}_4^+$  spin systems together with the possibility of obtaining  $^{15}\text{N}$ - $^1\text{H}$  correlation maps of protein-bound  $^{15}\text{NH}_4^+$  open up the possibility of quantifying the dynamics of ammonium ions, even within potassium binding-sites of large proteins, and thus for correlating cation

E-mail address: [d.hansen@ucl.ac.uk](mailto:d.hansen@ucl.ac.uk)

dynamics with macromolecular function. Given the current development of techniques to probe ammonium ions in proteins and nucleic acids it is therefore of interest to derive methods to experimentally measure nuclear spin-relaxation rates to report on the rotational correlation time and chemical exchange of ammonium ions. The advantage of the  $^{15}\text{NH}_4^+$  spin system is the availability of a wealth of coherences and spin density elements, whose relaxation rates each report differently on the rotational correlation time and chemical exchange. Herein NMR pulse sequences are developed firstly to select different spin density matrix elements and secondly to measure  $^{15}\text{N}$ -based longitudinal relaxation rates of the  $^{15}\text{NH}_4^+$  spin system. Applications to  $^{15}\text{N}$ -ammonium in an acidic aqueous solution and  $^{15}\text{N}$ -ammonium bound in a potassium binding-site of a  $\sim 41$  kDa domain of the protein DnaK are presented to illustrate the general utility of the derived pulse sequences.

## 2. Theory

*Time-evolution of the  $^{15}\text{NH}_4^+$  spin systems:* The time evolution of a spin system is generally given by the Liouville-von-Neumann equation [23–25]:

$$\frac{d\sigma(t)}{dt} = -i[\hat{\mathcal{H}}_0, \sigma(t)] - \Gamma(\sigma(t) - \sigma_{\text{eq}}) \quad (1)$$

where  $\hat{\mathcal{H}}_0$  is the time independent part of the spin-Hamiltonian,  $\sigma_{\text{eq}}$  is the equilibrium density operator, and  $\Gamma$  is the spin-relaxation super-operator, which was derived previously for the  $^{15}\text{N}$ -ammonium spin-system [20]. The time-independent part of the Hamiltonian is here given by:

$$\hat{\mathcal{H}}_0 = \hat{\mathcal{H}}_Z + \hat{\mathcal{H}}_J \quad (2)$$

$$\frac{d}{dt} \begin{pmatrix} N_+ \\ 2N_+ \mathbf{H}_z \\ 4N_+ \mathbf{H}_z \mathbf{H}_z \\ 8N_+ \mathbf{H}_z \mathbf{H}_z \mathbf{H}_z \\ 16N_+ \mathbf{H}_z \mathbf{H}_z \mathbf{H}_z \mathbf{H}_z \\ N_+ \mathbf{H}_+ \mathbf{H}_- \\ 2N_+ \mathbf{H}_+ \mathbf{H}_- \mathbf{H}_z \\ 4N_+ \mathbf{H}_+ \mathbf{H}_- \mathbf{H}_z \mathbf{H}_z \\ N_+ \mathbf{H}_+ \mathbf{H}_- \mathbf{H}_+ \mathbf{H}_- \end{pmatrix} = i\pi J \begin{pmatrix} 0 & 4 & 0 & 0 & 0 & 0 & 0 & 0 & 0 \\ 1 & 0 & 3 & 0 & 0 & 0 & 0 & 0 & 0 \\ 0 & 2 & 0 & 2 & 0 & 0 & 0 & 0 & 0 \\ 0 & 0 & 3 & 0 & 1 & 0 & 0 & 0 & 0 \\ 0 & 0 & 0 & 4 & 0 & 0 & 0 & 0 & 0 \\ 0 & 0 & 0 & 0 & 0 & 0 & 2 & 0 & 0 \\ 0 & 0 & 0 & 0 & 0 & 1 & 0 & 1 & 0 \\ 0 & 0 & 0 & 0 & 0 & 0 & 2 & 0 & 0 \\ 0 & 0 & 0 & 0 & 0 & 0 & 0 & 0 & 0 \end{pmatrix} \begin{pmatrix} N_+ \\ 2N_+ \mathbf{H}_z \\ 4N_+ \mathbf{H}_z \mathbf{H}_z \\ 8N_+ \mathbf{H}_z \mathbf{H}_z \mathbf{H}_z \\ 16N_+ \mathbf{H}_z \mathbf{H}_z \mathbf{H}_z \mathbf{H}_z \\ N_+ \mathbf{H}_+ \mathbf{H}_- \\ 2N_+ \mathbf{H}_+ \mathbf{H}_- \mathbf{H}_z \\ 4N_+ \mathbf{H}_+ \mathbf{H}_- \mathbf{H}_z \mathbf{H}_z \\ N_+ \mathbf{H}_+ \mathbf{H}_- \mathbf{H}_+ \mathbf{H}_- \end{pmatrix} \quad (3)$$

where the total Zeeman Hamiltonian is,  $\hat{\mathcal{H}}_Z = (H_{z1} + H_{z2} + H_{z3} + H_{z4})\omega_{\text{H}} + N_z\omega_{\text{N}}$ , and the  $^{15}\text{N}$ - $^1\text{H}$  scalar-coupling Hamiltonian is given by  $\hat{\mathcal{H}}_J = \pi J(2H_{z1}N_z + 2H_{z2}N_z + 2H_{z3}N_z + 2H_{z4}N_z)$ , and  $J$  is the nitrogen-proton one-bond scalar coupling constant.

As shown previously, there are nine single quantum  $^{15}\text{N}$  transitions within the tetrahedral  $^{15}\text{NH}_4^+$  spin system, however, due to the tetrahedral symmetry and degeneracy of the  $^{15}\text{NH}_4^+$  spin system there are only five characteristic frequencies of the single quantum  $^{15}\text{N}$  coherences:  $-4\pi J + \Omega$ ,  $-2\pi J + \Omega$ ,  $\Omega$ ,  $2\pi J + \Omega$ ,  $4\pi J + \Omega$ , where  $\Omega$  is the offset from the RF carrier. The frequency of a  $^{15}\text{N}$  transition depends on the spin states of the four ammonium protons, for example, when all the protons are in the  $\alpha$  state, the frequency is  $4\pi J + \Omega$ . In turn, the spin state of the four protons can be described using different basis sets; for example a Zeeman basis given by the eigenfunctions to the Zeeman Hamiltonian or a Cartesian basis. In the Zeeman basis set the transitions fall in three spin manifolds,  $A_1$ ,  $T_2$ , and  $E$  according to the  $T_d$  symmetry of the

ammonium ion as discussed previously [20]. For the development of the pulse sequence below the spin densities of the four ammonium protons are most conveniently described using the product operator formalism [26] and the Cartesian basis set.

In the product operator formalism the equilibrium density operator of the ammonium ion is given by  $\sigma_{\text{eq}} \propto \gamma_{\text{H}}(H_{z1} + H_{z2} + H_{z3} + H_{z4}) + \gamma_{\text{N}}N_z$ , where  $\gamma_{\text{H}}$  and  $\gamma_{\text{N}}$  are the gyromagnetic ratio of the proton and the nitrogen nuclear spin, respectively, and  $H_{zi}$  ( $i = 1, 2, 3, 4$ ) and  $N_z$  are the Cartesian product operator describing the longitudinal magnetisation of the four protons and the nitrogen spin, respectively. The transverse nitrogen magnetisation is written as  $N_+ = N_x + iN_y$ , where  $i$  is the imaginary unit. Thus, using the product operator formalism the nine single quantum nitrogen transitions are described by  $\mathcal{B}_{\text{xyz}} = \{N_+, 2N_+ \mathbf{H}_z, 4N_+ \mathbf{H}_z \mathbf{H}_z, 8N_+ \mathbf{H}_z \mathbf{H}_z \mathbf{H}_z, 16N_+ \mathbf{H}_z \mathbf{H}_z \mathbf{H}_z \mathbf{H}_z, N_+ \mathbf{H}_+ \mathbf{H}_-, 2N_+ \mathbf{H}_+ \mathbf{H}_- \mathbf{H}_z, 4N_+ \mathbf{H}_+ \mathbf{H}_- \mathbf{H}_z \mathbf{H}_z, N_+ \mathbf{H}_+ \mathbf{H}_- \mathbf{H}_+ \mathbf{H}_-\}$  in the Cartesian basis set, where the following notation has been used:  $\mathbf{H}_z = H_{z1} + H_{z2} + H_{z3} + H_{z4}$ ;  $\mathbf{H}_z \mathbf{H}_z = H_{z1}H_{z2} + H_{z1}H_{z3} + H_{z1}H_{z4} + H_{z2}H_{z3} + H_{z2}H_{z4} + H_{z3}H_{z4}$ ;  $\mathbf{H}_z \mathbf{H}_z \mathbf{H}_z = H_{z1}H_{z2}H_{z3} + H_{z1}H_{z2}H_{z4} + H_{z1}H_{z3}H_{z4} + H_{z2}H_{z3}H_{z4}$ ;  $\mathbf{H}_z \mathbf{H}_z \mathbf{H}_z \mathbf{H}_z = H_{z1}H_{z2}H_{z3}H_{z4}$ ;  $\mathbf{H}_+ \mathbf{H}_- = \sum_{i \neq j} H_{+i}H_{-j}$ ;  $\mathbf{H}_+ \mathbf{H}_- \mathbf{H}_z = \sum_{i \neq j \neq k} H_{+i}H_{-j}H_{zk}$ ;  $\mathbf{H}_+ \mathbf{H}_- \mathbf{H}_z \mathbf{H}_z = \sum_{i \neq j \neq k \neq l} H_{+i}H_{-j}H_{+k}H_{-l}$ . The advantage of using the Cartesian basis set here is that spin density elements present during the pulse sequence are more easily identified and the relaxation of the proton spins by external sources is conveniently implemented as additions to the auto-relaxation rates as described previously [20].

The evolution of spin density matrix elements under the scalar coupling Hamiltonian forms the basis for a separation of different nitrogen single quantum coherences. It is therefore of interest to characterise how the spin density elements of the basis  $\mathcal{B}_{\text{xyz}}$  evolve under the scalar coupling Hamiltonian. Only considering scalar coupling and ignoring relaxation, it was shown previously that [20]

Firstly it is noted that, due to the symmetry of the ammonium ion, the scalar coupling Hamiltonian is only mixing coherences within three groups:  $\{N_+, 2N_+ \mathbf{H}_z, 4N_+ \mathbf{H}_z \mathbf{H}_z, 8N_+ \mathbf{H}_z \mathbf{H}_z \mathbf{H}_z, 16N_+ \mathbf{H}_z \mathbf{H}_z \mathbf{H}_z \mathbf{H}_z\}$ ,  $\{N_+ \mathbf{H}_+ \mathbf{H}_-, 2N_+ \mathbf{H}_+ \mathbf{H}_- \mathbf{H}_z, 4N_+ \mathbf{H}_+ \mathbf{H}_- \mathbf{H}_z \mathbf{H}_z\}$ , and  $N_+ \mathbf{H}_+ \mathbf{H}_- \mathbf{H}_+ \mathbf{H}_-$  ( $N_+ \mathbf{H}_+ \mathbf{H}_- \mathbf{H}_+ \mathbf{H}_-$  commutes with the scalar coupling Hamiltonian). Thus, starting from in-phase transverse nitrogen magnetisation,  $N_x$ , gives:

$$\begin{aligned} N_x \xrightarrow{\tau 2\pi J N_z} & \frac{1}{8} (3 + 4 \cos 2\pi J \tau + \cos 4\pi J \tau) N_x + \frac{1}{8} (2 \sin 2\pi J \tau \\ & + \sin 4\pi J \tau) 2N_y \mathbf{H}_z - \frac{1}{8} (1 - \cos 4\pi J \tau) 4N_x \mathbf{H}_z \mathbf{H}_z \\ & - \frac{1}{8} (2 \sin 2\pi J \tau - \sin 4\pi J \tau) 8N_y \mathbf{H}_z \mathbf{H}_z \mathbf{H}_z \\ & + \frac{1}{8} (3 - 4 \cos 2\pi J \tau + \cos 4\pi J \tau) 16N_x \mathbf{H}_z \mathbf{H}_z \mathbf{H}_z \mathbf{H}_z \end{aligned} \quad (4)$$

Eq. (4) implies that evolution of  $N_x$  for a period of  $1/(2J)$  generates the quadruple anti-phase coherence  $16N_x \mathbf{H}_z \mathbf{H}_z \mathbf{H}_z \mathbf{H}_z$ . Moreover,

because the single anti-phase coherence,  $2N_{x,y}\mathbf{H}_z$ , is easily generated from the equilibrium density operator it's time evolution is also of particular interest here:

$$2N_x\mathbf{H}_z \xrightarrow{\tau 2\pi\mathbf{H}_z N_z} \frac{1}{2}(2 \sin 2\pi J\tau + \sin 4\pi J\tau)N_y + \frac{1}{2}(\cos 2\pi J\tau + \cos 4\pi J\tau)2N_x\mathbf{H}_z + \frac{1}{2}(\sin 4\pi J\tau)4N_y\mathbf{H}_z\mathbf{H}_z - \frac{1}{2}(\cos 2\pi J\tau - \cos 4\pi J\tau)8N_x\mathbf{H}_z\mathbf{H}_z\mathbf{H}_z - \frac{1}{2}(2 \sin 2\pi J\tau - \sin 4\pi J\tau)16N_y\mathbf{H}_z\mathbf{H}_z\mathbf{H}_z\mathbf{H}_z \quad (5)$$

Eqs. (4) and (5) imply that by choosing appropriate values of  $\tau$  in a pulse sequence a series of different coherences can be generated by evolving either in-phase transverse  $N_x$  magnetisation or the single anti-phase coherence  $2N_x\mathbf{H}_z$ .

It should be noted that inclusion of proton spin-flip,  $R_1(\mathbf{H}_z)$ , in the evolution described in Eq. (3) causes differential relaxation of the  $^{15}\text{N}$  single quantum Cartesian density elements and can effectively be viewed as a five-site exchange between the transitions of the  $^{15}\text{NH}_4^+$  multiplet. Thus, the signal with a frequency of  $-4\pi J + \Omega$  exchanges magnetisation with the signal at  $-2\pi J + \Omega$ , the signal with a frequency of  $-2\pi J + \Omega$  exchanges with the signals at  $-4\pi J + \Omega$  and at  $\Omega$ , and so forth. The consequence of proton spin-flip can therefore be a change in the characteristic frequencies, linewidths and intensities, which in turn can be calculated from the eigenvalues and eigenvectors of a Liouvillian that includes both the scalar coupling and proton spin-flip,  $R_1(\mathbf{H}_z)$ . It can be shown that inclusion of  $R_1(\mathbf{H}_z)$  in the Liouvillian, and assuming that  $R_1(\mathbf{H}_z) < 2\pi|J|$ , changes the characteristic frequencies to  $\{-4\pi J[1 - \zeta^2]^{1/2} + \Omega, -2\pi J[1 - \zeta^2]^{1/2} + \Omega, \Omega, 2\pi J[1 - \zeta^2]^{1/2} + \Omega, 4\pi J[1 - \zeta^2]^{1/2} + \Omega\}$ , where  $\zeta = R_1(\mathbf{H}_z)/(2\pi J)$ . Moreover, when the single anti-phase coherence  $2N_x\mathbf{H}_z$  is excited and detected, for example in a standard coupled  $^{15}\text{N}$ - $^1\text{H}$  correlation spectrum, the intensity ratio of the five signals is 1:r:0:r:1, with  $r = 1 - 5\zeta(\zeta - \frac{4\pi}{5}\sqrt{1 - \zeta^2})$ . For experimental spectra of  $^{15}\text{NH}_4^+$  the effects on the frequencies and the intensity ratios are generally small. For example, when  $J = -70$  Hz and  $R_1(\mathbf{H}_z) = 35$  s $^{-1}$ , which is well within the range of the data shown below, the characteristic frequencies are  $\{-139.56$  Hz,  $-69.79$  Hz,  $0$  Hz,  $69.79$  Hz,  $139.56$  Hz $\}$  and the absolute intensity ratio is 1:1.02:0:1.02:1. It should be noted that since  $r$  is a complex number, the proton spin-flip also causes a relative phase-shift of the signals within the multiplet, as also observed previously for two-site chemical exchange [27]; this phase-shift is approximately  $10^\circ$  for the example above.

### 3. Results

*Pulse sequence for measuring the longitudinal relaxation rates of  $^{15}\text{NH}_4^+$ :*  $^{15}\text{N}$ -ammonium ions in an acid aqueous solution or bound to proteins or nucleic acids can be characterised by  $^{15}\text{N}$ - $^1\text{H}$  correlations spectra [17–20]. Such two-dimensional spectra can be obtained using standard  $^{15}\text{N}$ - $^1\text{H}$  correlation experiments, where after an initial INEPT,  $90_x(^1\text{H}) - \tau - 180_x(^1\text{H}), 180_x(^{15}\text{N}) - \tau - 90_y(^1\text{H})$  with  $\tau = 1/(4J)$ , a spin density operator proportional to  $2N_z\mathbf{H}_z$  is generated. Subsequently a  $90_x(^{15}\text{N})$  pulse generates  $-2N_y\mathbf{H}_z$  for chemical shift evolution and a final INEPT transfers anti-phase  $2N_{x,y}\mathbf{H}_z$  magnetisation to transverse proton magnetisation for detection. When the  $^{15}\text{N}$ - $^1\text{H}$  scalar coupling is allowed to evolve during the  $2N_{x,y}\mathbf{H}_z$  chemical shift evolution period signals at the five  $^{15}\text{N}$  characteristic frequencies  $-4\pi J + \Omega, -2\pi J + \Omega, \Omega, 2\pi J + \Omega$ , and  $4\pi J + \Omega$  (Eq. (5)) are observed with an intensity ratio of 1:1:0:1:1 [20] in the limit where  $R_1(^1\text{H}) \lesssim 2\pi|J|$  (see Section 2). The pulse sequence used here for generating subspectra of the  $^{15}\text{NH}_4^+$  quintet and for measuring relaxation rates of the longitudinal density operator elements is shown in Fig. 1 and is based on the  $^{15}\text{N}$ - $^1\text{H}$  correlation experiment described above.

The sequence in Fig. 1 differs from a standard  $^{15}\text{N}$ - $^1\text{H}$  correlation experiment by the insertion of a selection element between *a* and *b* and a relaxation delay prior to the  $^{15}\text{N}$  chemical shift evolution. The final INEPT between *c* and acquisition selects for the two spin-order longitudinal spin density element,  $2N_z\mathbf{H}_z$ , and transfers it to  $\mathbf{H}_y$  magnetisation for detection while a pair of  $^{15}\text{N}$   $90^\circ$  pulses, with the first pulse phase-cycled  $x, -x$ , is placed immediately prior to acquisition to remove anti-phase  $2N_z\mathbf{H}_{xy}$  coherences.

*Selecting subspectra of the  $^{15}\text{NH}_4^+$  quintet:* The initial  $90_{\phi_1}^{15}\text{N}$  pulse of the selection element between *a* and *b* in Fig. 1 generates the  $\pm 2N_y\mathbf{H}_z$  anti-phase spin density element. Free precession of  $2N_y\mathbf{H}_z$  during the coherence selection element can be characterised schematically using a vector model, where each of the four observed signals of the  $^{15}\text{NH}_4^+$  quintet are represented by a vector (Fig. 2). A  $^{15}\text{N}$   $180^\circ$  pulse is applied in the middle of the coherence selection element such that chemical shift evolution of  $^{15}\text{N}$  is refocused. Relaxation during the selection element is disregarded initially and therefore only the evolution under the  $^{15}\text{N}$ - $^1\text{H}$  scalar coupling Hamiltonian is considered immediately below.

The selection element shown in the pulse sequence of Fig. 1 relies on both a variation of the delay  $\tau_b$  and on the phase  $\phi_4$ . In the limiting case when  $\tau_b = \tau_a$  the evolution under the scalar coupling Hamiltonian is refocused, while when  $\tau_b = 0$  the scalar coupling evolves for  $1/|2J|$  and a spin density element proportional to  $8N_z\mathbf{H}_z\mathbf{H}_z$  is obtained (Eq. (5)). For other values of  $\tau_b$  the evolution of the scalar coupling can conveniently be followed using a

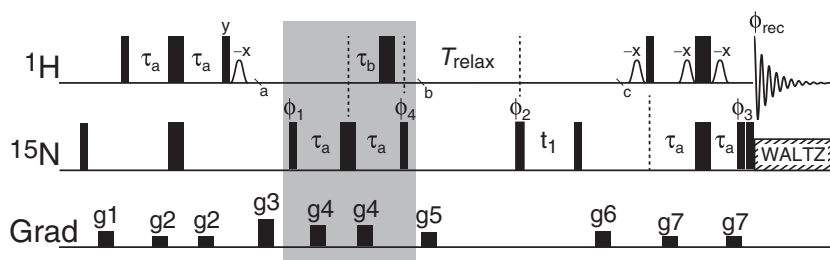


**Fig. 1.** Pulse sequence to measure longitudinal relaxation rates of individual spin density matrix elements of the  $^{15}\text{NH}_4^+$  spin-system. The  $^1\text{H}$  carrier is placed on the water and the  $^{15}\text{N}$  carrier is placed in the middle of the  $^{15}\text{NH}_4^+$  region ( $\sim 20$  ppm). All pulses are applied at the highest possible power levels, with the exception of the  $^1\text{H}$  water selective pulses (open bell-shaped pulses) and the  $^{15}\text{N}$  decoupling, where a  $\sim 350$  Hz field strength and a 1.5 kHz WALTZ-16 decoupling [28] are employed, respectively. The element immediately following the initial INEPT (grey box) is used to select different coherences of the  $^{15}\text{NH}_4^+$  spin system, as detailed in the text. The delay used are:  $\tau_a = 3.47$  ms and  $\tau_b$  varied as described in the main text. Pulses without annotation are applied with  $x$ -phase. The phase cycle is:  $\phi_1 = x, -x, \phi_2 = 2(x), 2(-x), \phi_3 = 4(x), 4(-x), \phi_{\text{rec}} = x, -x, -x, x$ . The phase of  $\phi_4$  is chosen as a part of the coherence selection element and detailed in the text and in Fig. 3. Quadrature detection in the indirect  $^{15}\text{N}$  dimension is achieved by altering  $\phi_2$  and  $\phi_{\text{rec}}$  in the States-TPPI manner. Gradients are used to remove artifacts and are applied using a sine bell-shaped profile for 0.5 ms with maximum strengths of, g1: 24 G/cm, g2: 7.3 G/cm, g3: 35 G/cm, g4: 15 G/cm, g5: 8.6 G/cm, g6: 11.2 G/cm, g7: 8.6 G/cm.

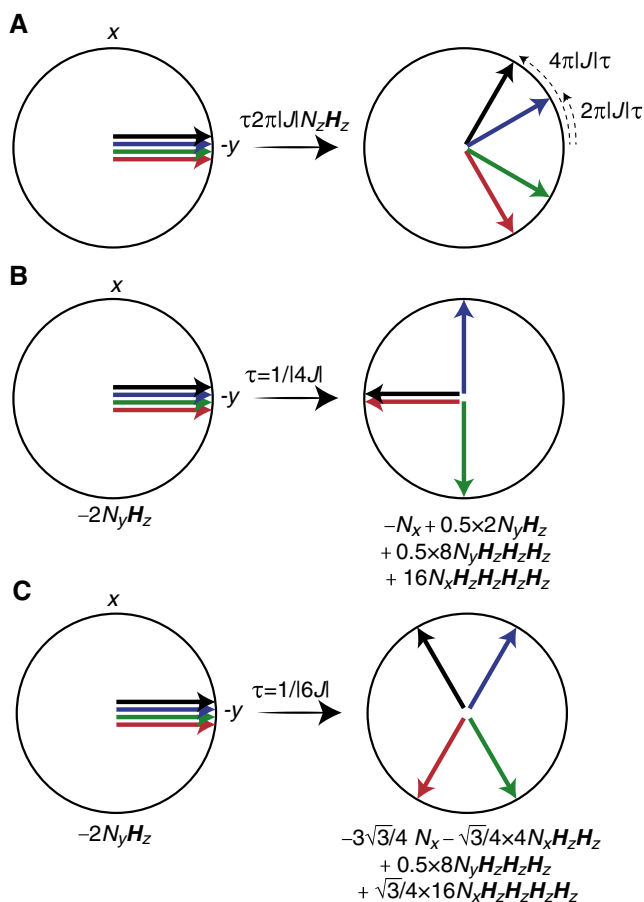


**Fig. 2.** (A) Vector diagram showing the evolution of transverse  $^{15}\text{N}$  magnetisations of the  $^{15}\text{NH}_4^+$  spin-system under the  $^{15}\text{N}$ - $^1\text{H}$  scalar coupling Hamiltonian. The vectors correspond to the four transitions observed in the coupled  $^{15}\text{N}$  spectrum that is obtained by exciting and detecting the anti-phase coherence  $2N_xH_z$ . Specifically, the red vector corresponds to the transition where all the ammonium protons are in the  $\alpha$ -state, green vector corresponds to the transitions where three of the protons are in the  $\alpha$ -state, blue vector corresponds to the transitions where one of the protons is in the  $\alpha$ -state, and black vector corresponds to the situation where all the protons are in the  $\beta$ -state. (B) Evolution of the anti-phase coherence  $-2N_yH_z$  under the scalar coupling Hamiltonian for a time of  $|1/4J|$  ( $J < 0$  for  $^{15}\text{N}$ - $^1\text{H}$  scalar couplings). Selection along the  $y$ -axis generates an intensity ratio of 0:–1:0:1:0 of the five  $^{15}\text{N}$  characteristic frequencies and a spin density element proportional to  $N_z - 16N_xH_zH_zH_zH_z$ , while selection along the  $x$ -axis generates an intensity ratio of 1:0:0:0:1 of the five  $^{15}\text{N}$  characteristic frequencies and a spin density element proportional to  $2N_xH_z + 8N_xH_zH_zH_zH_z$ . (C) Evolution of the anti-phase coherence  $-2N_yH_z$  under the scalar coupling Hamiltonian for a time of  $|1/6J|$ . Selection along the  $y$ -axis generates an intensity ratio of 1:1:0:–1:–1 of the five  $^{15}\text{N}$  characteristic frequencies, while selection along the  $x$ -axis generates an intensity ratio of 1:–1:0:–1:1 of the five  $^{15}\text{N}$  characteristic frequencies.

vector diagram as shown in Fig. 2A. Specifically, Fig. 2B and C show the selection of four different spin density elements of the  $^{15}\text{NH}_4^+$  spin-system. It should be noted that differential relaxation of the density elements  $\{N_+, 2N_+H_z, \dots, 16N_+H_zH_zH_zH_z\}$  during the selection element becomes significant for application to  $^{15}\text{NH}_4^+$  systems with large proton spin-flip rates,  $R_1(H_z)$ . As discussed below the effect of differential relaxations can be taken into account in the analysis of relaxation decay curves by introducing model parameters that describe the state immediately following the selection element.

The pulse sequence in Fig. 1 and the selection element were initially verified using  $^{15}\text{NH}_4^+$  in an acidic aqueous solution. Under acidic conditions (pH = 2.82) the exchange rate of the ammonium protons with the water is slowed to an extent where  $^{15}\text{N}$ - $^1\text{H}$  correlation spectra can be obtained and where the pulse sequence in Fig. 1 can be verified. Fig. 3 shows the generation of four different

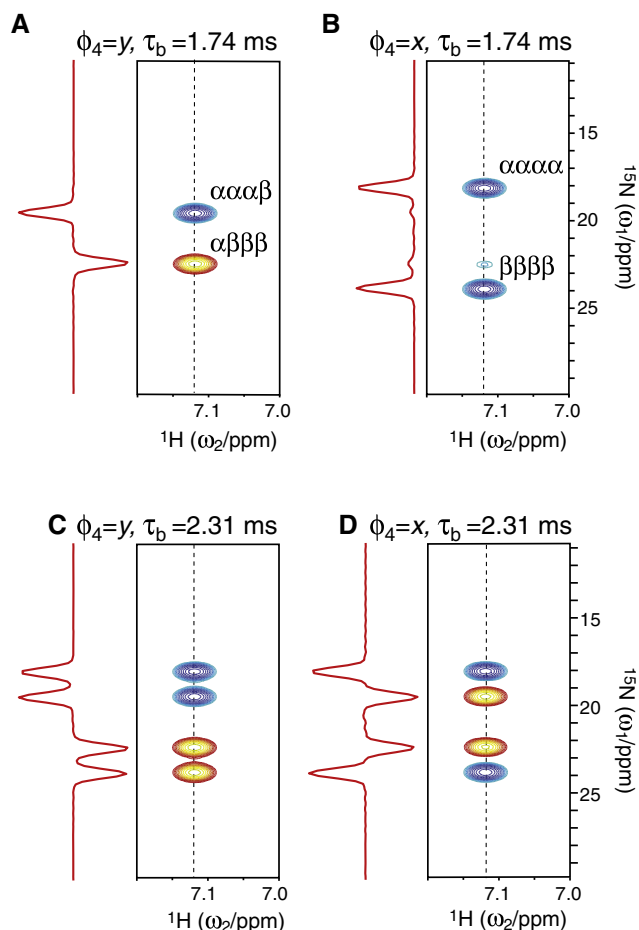


**Fig. 3.** Selection of spin density matrix elements of  $^{15}\text{NH}_4^+$  dissolved in an acidic aqueous solution (pH = 2.82). The spectra were obtained using the sequence shown in Fig. 1, with  $T_{\text{relax}} = 0$  and  $\tau_b$  and  $\phi_4$  as shown above each of the panels. (A) The selection of  $N_x - 16N_xH_xH_xH_xH_x$  coherences; corresponding to Fig. 2B with selection along  $x$ . (B) The selection of  $2N_xH_x + 8N_xH_xH_xH_xH_x$  coherences; corresponding to Fig. 2B with selection along the  $y$ -axis. (C) and (D) Selection shown in Fig. 2C with selection phase along the  $x$ - and  $y$ -axis, respectively.

spectra obtained by varying  $\tau_b$  and  $\phi_4$ . The obtained spectra are in excellent agreement with the predicted ratio of the intensities of the multiplet structure.

Linear combinations of the spectra in Fig. 3 can be used to generate spectra of four of the individual lines of the  $^{15}\text{NH}_4^+$  quintet, where for example, the spectra in Fig. 3A–C can be used to generate a spectrum only consisting of the  $\alpha\alpha\alpha\alpha$  line. It should be noted however that although spectra of the four lines can be generated, pure spectra of all of the five Cartesian  $^{15}\text{N}$  single quantum spin density elements,  $N_+, 2N_+H_z, \dots, 16N_+H_zH_zH_zH_z$ , cannot be generated using the described sequence. A spectrum of pure  $2N_xH_x$  and pure  $8N_xH_xH_xH_xH_x$  can be generated from Fig. 3B and D, or from spectra with  $\tau_b = \tau_a$  and  $\tau_b = 0$  s, respectively. A further consequence is that the intensity of the four lines,  $\alpha\alpha\alpha\alpha$ ,  $\alpha\alpha\alpha\beta$ ,  $\alpha\beta\beta\beta$ , and  $\beta\beta\beta\beta$  can be used to derive the relative intensity of  $2N_xH_x$  and  $8N_xH_xH_xH_xH_x$ . On the contrary, the pure spectra corresponding to the three spin density elements  $N_+, 4N_xH_xH_xH_xH_x$ , and  $16N_+H_zH_zH_zH_z$  are correlated such that their individual intensities cannot be separated using the selection elements in Fig. 1. Such a correlation is the result of an underdetermined system where four lines are observed in the coupled  $^{15}\text{N}$ - $^1\text{H}$  NMR spectra, however originating from five spin density elements. On the other hand, when the contributions from the five possible spin density elements are known, the intensities of the four lines can be calculated.

**Measuring longitudinal relaxation rates:** In general, the relaxation rate of the five longitudinal spin density elements,  $N_z$ ,  $2N_z\mathbf{H}_z$ ,  $4N_z\mathbf{H}_z\mathbf{H}_z$ ,  $8N_z\mathbf{H}_z\mathbf{H}_z\mathbf{H}_z$  and  $16N_z\mathbf{H}_z\mathbf{H}_z\mathbf{H}_z\mathbf{H}_z$  are different, since they have different contributions from the spectral density function  $J(\omega)$  and different contributions from the proton spin-flip rate,  $R_1(\mathbf{H}_z)$  [20]. When the rotational diffusion of the  $^{15}\text{NH}_4^+$  ion is described accurately by one correlation time,  $\tau_c$ , the five relaxation rates,  $R_1(N_z)$ ,  $R_1(2N_z\mathbf{H}_z)$ ,  $R_1(4N_z\mathbf{H}_z\mathbf{H}_z)$ ,  $R_1(8N_z\mathbf{H}_z\mathbf{H}_z\mathbf{H}_z)$ , and  $R_1(16N_z\mathbf{H}_z\mathbf{H}_z\mathbf{H}_z\mathbf{H}_z)$ , as well as cross-correlated relaxations between the longitudinal spin density elements, only depend on two parameters, that is, the rotational correlation time  $\tau_c$  and the proton spin-flip rate,  $R_1(\mathbf{H}_z)$ . Thus, as described below using the Liouvillian in Table 4 of Werbeck and Hansen [20], which includes both auto- and cross-correlated relaxations, the two parameters  $\tau_{c,\text{eff}}$  and  $R_1(\mathbf{H}_z)$  can be obtained from the intensities of the four lines observed in coupled  $^{15}\text{NH}_4^+$  spectra recorded for different values  $T_{\text{relax}}$ .

A relaxation delay,  $T_{\text{relax}}$ , is inserted after the selection element and before the  $^{15}\text{N}$  chemical shift evolution in the sequence in Fig. 1, which allows the relaxation decay of the four lines ( $\alpha\alpha\alpha\alpha$ ,  $\alpha\alpha\alpha\beta$ ,  $\alpha\beta\beta\beta$ ,  $\beta\beta\beta\beta$ ) to be obtained in order to characterise the dynamics of the ammonium ion. Initially  $^{15}\text{NH}_4^+$  in acidic aqueous solutions (pH 2.82) was used as a model system. For such a system the proton spin-flip rate  $R_1(\mathbf{H}_z)$  is given by the off-rate of the ammonium protons with the bulk solvent:  $^{15}\text{NH}_4^+ + \text{H}_2\text{O} \xrightarrow{k_{\text{off}}} ^{15}\text{NH}^+\text{H}_3^+ + \text{H}^+\text{OH}$ .

Although there are many possible combinations of  $\tau_b$  and  $\phi_4$ , each allowing for a different selection of spin density elements, focus below is on selecting two initial states, that is (i)  $2N_z\mathbf{H}_z + 8N_z\mathbf{H}_z\mathbf{H}_z\mathbf{H}_z$  and (ii)  $N_z - 16N_z\mathbf{H}_z\mathbf{H}_z\mathbf{H}_z\mathbf{H}_z$ . The decay curves obtained for  $^{15}\text{NH}_4^+$  in an acidic aqueous solution following these two different selections is shown in Fig. 4. It is noted that in the logarithmic plots the decay curves show a double sigmoidal shape reporting on the relaxation of the different spin density elements present during the relaxation delay. For example, for the selection of an element proportional to  $N_z - 16N_z\mathbf{H}_z\mathbf{H}_z\mathbf{H}_z\mathbf{H}_z$  the faster relaxation of  $16N_z\mathbf{H}_z\mathbf{H}_z\mathbf{H}_z\mathbf{H}_z$  is seen by the first sigmoidal shape and thereafter the relative ratio of the intensity of the four observed lines approaches the 1:2:0:–2 ratio that is characteristic for the in-phase magnetisation. Similarly, for selection of an initial spin density element proportional to  $2N_z\mathbf{H}_z + 8N_z\mathbf{H}_z\mathbf{H}_z\mathbf{H}_z\mathbf{H}_z$  the ratio of the intensity of the four signals approaches 1:1:0:1:1, which is characteristic of the single anti-phase coherence  $2N_z\mathbf{H}_z$ .

The decay curves were analysed by evolution of the Liouvillian in the Cartesian basis,  $\Gamma$ , during the relaxation delay  $T_{\text{relax}}$ . Here the Liouvillian is a function of the two parameters  $\tau_c$  and  $R_1(\mathbf{H}_z)$  and describes the auto- and cross-correlated relaxation rates within the basis set  $\{E/2, \mathbf{H}_z, 2\mathbf{H}_z\mathbf{H}_z, 4\mathbf{H}_z\mathbf{H}_z\mathbf{H}_z, 8\mathbf{H}_z\mathbf{H}_z\mathbf{H}_z\mathbf{H}_z, N_z, 2N_z\mathbf{H}_z, 4N_z\mathbf{H}_z\mathbf{H}_z, 8N_z\mathbf{H}_z\mathbf{H}_z\mathbf{H}_z, 16N_z\mathbf{H}_z\mathbf{H}_z\mathbf{H}_z\mathbf{H}_z\}$ . Using a larger basis set that includes also the zero-quantum density elements such as  $N_z\mathbf{H}_z\mathbf{H}_z$  and  $2N_z\mathbf{H}_z\mathbf{H}_z$ , did not change the quality of the fit nor did it change the obtained parameters. Briefly, a vector describing the initial state  $\mathbf{v}_0 = \{0, 0, 0, 0, 0, I_0(N_z), I_0(2N_z\mathbf{H}_z), I_0(4N_z\mathbf{H}_z\mathbf{H}_z), I_0(8N_z\mathbf{H}_z\mathbf{H}_z\mathbf{H}_z), I_0(16N_z\mathbf{H}_z\mathbf{H}_z\mathbf{H}_z\mathbf{H}_z)\}$  was evolved for a time of  $T_{\text{relax}}$ . The intensity of the density elements,  $E/2, \mathbf{H}_z, 2\mathbf{H}_z\mathbf{H}_z, 4\mathbf{H}_z\mathbf{H}_z\mathbf{H}_z$ , and  $8\mathbf{H}_z\mathbf{H}_z\mathbf{H}_z\mathbf{H}_z$  were assumed to vanish, because phase  $\phi_1$  in the pulse sequence of Fig. 1 is phase-cycled  $\{x, -x\}$  with no concomitant change in the receiver phase, which eliminates contributions from density elements not proportional to  $N_z$  or  $N_y$ . After evolving the initial state  $\mathbf{v}_0$  for a time of  $T_{\text{relax}}$  the intensities of  $\mathbf{v}(T_{\text{relax}})$  were converted to intensities of the four lines observed,  $\{I_{\alpha\alpha\alpha\alpha}, I_{\alpha\alpha\alpha\beta}, I_{\alpha\beta\beta\beta}, I_{\beta\beta\beta\beta}\}$ . The best-fit model parameters,  $\tau_c$ ,  $R_1(\mathbf{H}_z)$ , and  $\mathbf{v}_0$ , were subsequently obtained by a Levenberg-Marquardt least-squared fitting procedure (see Section 5).

Analysis of the decay curves in Fig. 4 gives a correlation time of  $\tau_c = 1.63 \text{ ps} \pm 0.03 \text{ ps}$  and  $R_1(\mathbf{H}_z) = 4.34 \text{ s}^{-1} \pm 0.02 \text{ s}^{-1}$ . Moreover,

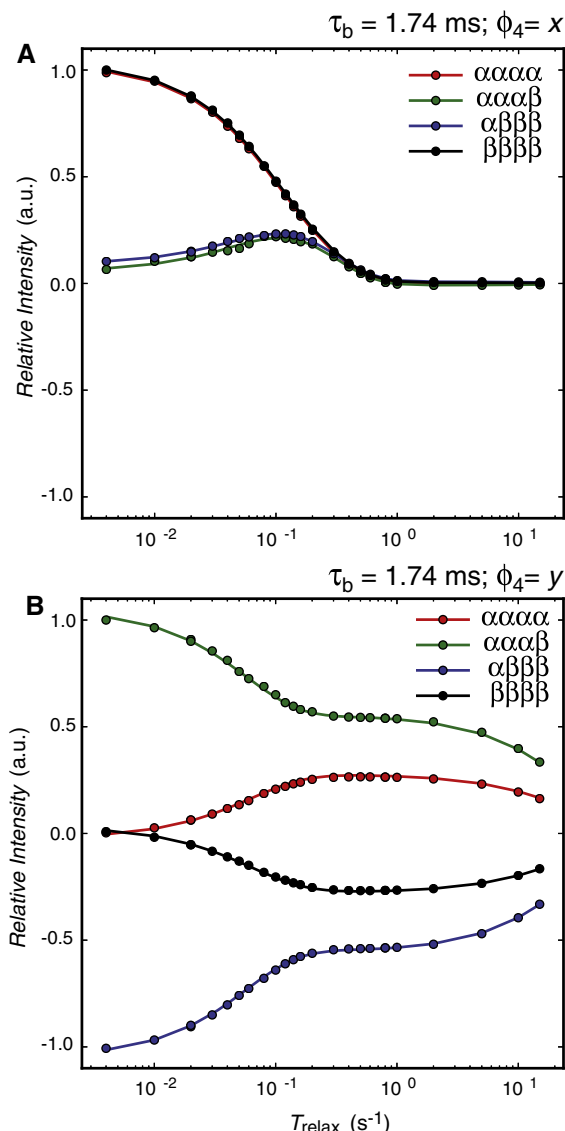


**Fig. 4.** Decay curves of the four lines observed in the coupled  $^{15}\text{NH}_4^+$  spectrum of  $^{15}\text{NH}_4^+$  in an acidic aqueous solution; pH 2.82 at 278 K, and recorded at a static magnetic field of 11.74 T. The solid lines are obtained from best-fits of all the data shown to an evolution of the Liouvillian describing the decay of the five Cartesian longitudinal spin density elements (see text). (A) Decay curves obtained after selecting for  $2N_z\mathbf{H}_z + 8N_z\mathbf{H}_z\mathbf{H}_z\mathbf{H}_z$  and using the pulse sequence of Fig. 1. (B) Decay curves obtained after selecting for  $N_z - 16N_z\mathbf{H}_z\mathbf{H}_z\mathbf{H}_z\mathbf{H}_z$ . The double sigmoidal shape of the decay curves in the logarithmic plot shows first the faster relaxation of the quadruple anti-phase spin density element  $16N_z\mathbf{H}_z\mathbf{H}_z\mathbf{H}_z\mathbf{H}_z$  followed by a substantially slower relaxation of the in-phase longitudinal magnetisation  $N_z$ .

the intensities obtained for the initial states were  $\mathbf{v}_0 = \{0, 0, 0, 0, 0, 0, 0.017 \pm 0.001, 0.552 \pm 0.001, 0.002 \pm 0.001, 0.480 \pm 0.001, 0.002 \pm 0.001\}$  for the data shown in Fig. 4A and  $\mathbf{v}_0 = \{0, 0, 0, 0, 0, -1.106 \pm 0.002, 0.003 \pm 0.001, 0.037 \pm 0.002, 0.002 \pm 0.001, 0.991 \pm 0.005\}$  for the data shown in Fig. 4B, respectively. It is seen that the obtained selection is very similar to the predicted selection, with  $I_0(2N_z\mathbf{H}_z)/I_0(8N_z\mathbf{H}_z\mathbf{H}_z\mathbf{H}_z) = 1.15$  (predicted value = 1) and  $I_0(N_z)/I_0(16N_z\mathbf{H}_z\mathbf{H}_z\mathbf{H}_z\mathbf{H}_z) = -1.12$  (predicted value = -1). The small deviation from the predicted values could be a result of relaxation during the selection element and if  $\tau_a$  is slightly different from  $1/|4J|$ .

In order to verify the obtained correlation time and proton spin-flip rate a second set of data was obtained at a static magnetic field strength of 16.44 T (700 MHz proton frequency). Here, the same two experiments were recorded as above, that is (i) selecting for

an initial state proportional to  $2N_zH_z + 8N_zH_zH_zH_z$  and (ii) selecting for an initial state proportional to  $N_z - 16N_zH_zH_zH_zH_z$ . The quality of the data obtained at 16.44 T are similar to those obtained at 11.74 T and simultaneous analysis of the two data set at 16.44 T gives  $\tau_c = 1.47 \text{ ps} \pm 0.04 \text{ ps}$  and  $R_1(H_z) = 4.32 \text{ s}^{-1} \pm 0.02 \text{ s}^{-1}$ . The spin-flip rate obtained at 16.44 T agrees extremely well with the spin-flip rate obtained at 11.74 T. Contributions from the  $^{15}\text{N}$  chemical shift anisotropy (CSA) relaxation mechanism to the relaxation rates are expected to vanish for the ammonium ion due to its tetrahedral symmetry. The slightly shorter correlation time obtained at 16.44 T compared to 11.74 T confirms that contributions from  $^{15}\text{N}$  CSA to the relaxation is negligible, since an  $^{15}\text{N}$  CSA contribution to the longitudinal relaxation rates would lead to larger relaxation rates at higher fields and thus an artificially too long correlation times being obtained at higher fields. Moreover, the correlation time obtained here is in good agreement with the rotational correlation time obtained previously from measurement of in-phase longitudinal  $R_1(N_z)$  relaxation rates of  $^{15}\text{N}$ -ammonium in water and at 276.5 K;  $\tau_c = 1.41 \text{ ps}$  [5].

**Application to  $^{15}\text{N}$ -ammonium bound to the 41kDa ATP binding domain of DnaK:** The pulse sequence of Fig. 1 together with the equations for the auto- and cross-correlated relaxation rates within the  $^{15}\text{NH}_4^+$  spin system provide the basis to characterise the local dynamics and chemical exchange properties of ammonium ions in various environments. The applications above to  $^{15}\text{N}$ -ammonium in an acidic aqueous solution provide the correlation time of the ammonium ion and thus provide a validation of the pulse sequence shown in Fig. 1 for the measurement of longitudinal relaxation rates of  $^{15}\text{NH}_4^+$  longitudinal spin density elements. The correlation time for ammonium ions in various solvents have been characterised [6], however the correlation time of ammonium ions within specific monovalent cation binding-sites in proteins have not been characterised previously. Previous applications [19,20] have shown that  $^{15}\text{N}$ -ammonium within potassium binding-sites in medium-large proteins can be probed using  $^{15}\text{N}$ - $^1\text{H}$  correlation spectra and the pulse sequence presented above in Fig. 1 therefore opens up for the possibility of measuring longitudinal relaxation rates of  $^{15}\text{N}$ -ammonium within potassium-binding sites in medium-large proteins.

The activity of the bacterial Hsp70 homologue DnaK relies on the binding of two potassium ions, where the two potassium ions in the ATP binding domain have been shown to be crucial for the ATP cycle [22]. Of interest here is that potassium can be substituted by ammonium with the enzyme retaining more than half of its activity [22]. Previous applications have shown that  $^{15}\text{N}$ -ammonium within the two potassium binding sites of a 41 kDa domain of DnaK can be probed using  $^{15}\text{N}$ - $^1\text{H}$  correlation spectra, when ADP and inorganic phosphate are added to create an environment that protects the ammonium ion from the bulk solvent. An initial application below to  $^{15}\text{N}$ -ammonium bound to one of the two potassium binding-sites in DnaK will illustrate the applicability of the method of measuring longitudinal relaxation rates of  $^{15}\text{N}$ -ammonium in medium-large proteins.

Selection of the initial state and measurements of longitudinal relaxation rates of  $^{15}\text{N}$ -ammonium in DnaK at 18.79 T (800 MHz proton frequency) and at 278 K is shown in Fig. 5.

As for the application to  $^{15}\text{N}$ -ammonium in acidic aqueous solutions shown above two relaxation experiments were carried out, that is, selecting for an initial state proportional to  $2N_zH_z + 8N_zH_zH_zH_z$  (Fig. 5A) and selecting for an initial state proportional to  $N_z - 16N_zH_zH_zH_zH_z$  (Fig. 5B). A simultaneous analysis of the two set of data and neglecting chemical exchange provides a proton spin-flip rate of  $R_1(H_z) = 19.7 \text{ s}^{-1} \pm 1.4 \text{ s}^{-1}$  and an effective correlation time of  $\tau_{c,\text{eff}} = 66.3 \pm 3.5 \text{ ps}$ . These model parameters correspond to auto-relaxation rates of

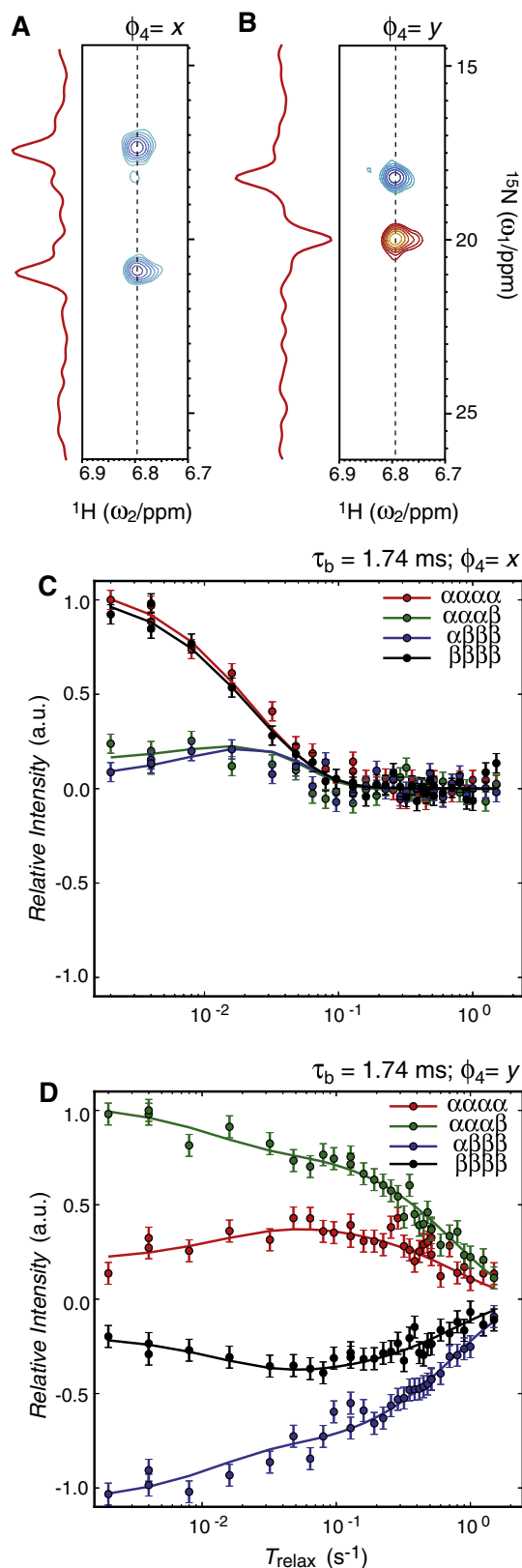


**Fig. 5.** Characterising  $^{15}\text{N}$  longitudinal relaxation of  $^{15}\text{NH}_4^+$  bond to a  $\sim 41$  kDa domain of DnaK at a field of 18.79 T and a temperature of 278 K. (A)  $^{15}\text{N}$ - $^1\text{H}$  correlation spectrum obtained after selecting for  $2N_zH_z + 8N_zH_zH_zH_z$ . (B)  $^{15}\text{N}$ - $^1\text{H}$  correlation spectrum obtained after selecting for  $N_z - 16N_zH_zH_zH_zH_z$  using the pulse sequence of Fig. 1. (C) Relaxation decay curve obtained following the selection in A. (D) Relaxation decay curve obtained following the selection in B. Shown in solid lines are the global fit of all the data shown in C and D.

$R_1(N_z) = 1.30 \pm 0.07 \text{ s}^{-1}$ ,  $R_1(2N_zH_z) = 26.6 \pm 1.5 \text{ s}^{-1}$ ,  $R_1(4N_zH_zH_z) = 48.6 \pm 2.9 \text{ s}^{-1}$ ,  $R_1(8N_zH_zH_zH_z) = 68.0 \pm 4.3 \text{ s}^{-1}$ , and  $R_1(16N_zH_zH_zH_zH_z) = 85.5 \pm 5.7 \text{ s}^{-1}$ . Moreover, the intensities obtained for the initial states are  $\mathbf{v}_0 = \{0, 0, 0, 0, 0, 0.028 \pm 0.027, 0.632 \pm 0.017, -0.018 \pm 0.024, 0.432 \pm 0.021, 0.011 \pm 0.077\}$  for the data shown in Fig. 5C and  $\mathbf{v}_0 = \{0, 0, 0, 0, 0, -1.693 \pm 0.040, 0.021 \pm 0.016, 0.091 \pm 0.026, -0.002 \pm 0.020, 0.276 \pm 0.086\}$  for the data shown in Fig. 5D, respectively. The large proton spin-flip rate causes relaxation during the selection element, such that the selections shown in Fig. 5A and B are not exactly proportional to  $2N_zH_z + 8N_zH_zH_zH_z$  and  $N_z - 16N_zH_zH_zH_zH_z$ , respectively. This becomes particularly apparent for the selection of  $N_z - 16N_zH_zH_zH_zH_z$  (Fig. 5B and D), where the fast relaxation of the quadruple anti-phase element leads to a ratio of  $I_0(16N_zH_zH_zH_zH_z)/I_0(N_z) \sim -0.16$  instead of  $-1$ . It should be stressed that a determination of the initial state is included in the least-squared analysis via the model parameter  $\mathbf{v}_0$  and as such the different selections serve merely as a means of providing initial states that are different enough to allow for an accurate determination of both  $R_1(H_z)$  and  $\tau_{C,\text{eff}}$ .

It is interesting to note that the effective rotational correlation time obtained here for the ammonium ion is very similar to the rotational correlation time of a methyl group within a protein environment, which has been found to be between  $25 \text{ ps} \lesssim \tau_{\text{Me}} \lesssim 125 \text{ ps}$ , depending on residue type and temperature [29–31]. A previous investigation of the dynamics of lysine side chains has shown that the correlation time for the rotation about the three-fold axis of the lysine  $\text{—NH}_3^+$  group reports on hydrogen bonding [32]. The potassium binding sites in DnaK are lined with negative charges from aspartic acid side chains and phosphate groups and hydrogen-bonding and/or salt-bridging is therefore possible and could explain the ca. 40 times longer correlation time for DnaK-bound ammonium compared to free ammonium.

It was assumed above that the rotational correlation function for  $^{15}\text{NH}_4^+$  bound to DnaK can be described accurately with one effective correlation time and chemical exchange events, for example dissociation of  $^{15}\text{NH}_4^+$  from the binding site, were neglected. The dependence of the  $^{15}\text{NH}_4^+$  longitudinal relaxation rates on temperature and the dependence of the rates on the static magnetic field strength are still to be explored. Such future explorations will, for example, give information about whether the correlation function for the rotational diffusion of ammonium ions bound to proteins is accurately described by one correlation time,  $\tau_{C,\text{eff}}$ , or if more elaborate models for the correlation function need to be employed. The temperature dependence of the derived relaxation rates will aid to elucidate possible chemical exchange events such as dissociation of the ammonium ion.

#### 4. Conclusions

In summary, NMR pulse schemes have been developed to both select different longitudinal spin density matrix elements of  $^{15}\text{N}$ -ammonium and also to obtain the longitudinal  $^{15}\text{N}$  relaxation rates of these longitudinal spin density elements. An initial application to  $^{15}\text{NH}_4^+$  in an acidic aqueous solution was used to validate the pulse scheme and the new method to derive the effective correlation time of the  $^{15}\text{NH}_4^+$  spin system.

An application of the derived pulse scheme to probe the dynamics of enzyme-bound ammonium ions was subsequently described, where in particular the possibility of characterising  $^{15}\text{N}$ -ammonium bound to a 41 kDa domain of DnaK at 278 K shows the very general applicability of the method. For such a system, the protein itself is expected to have a rotational correlation time of approximately 36 ns at 278 K, thus confirming that the derived method is applicable to characterise potassium binding-site in medium-large proteins.

The pulse scheme and method presented here provides an avenue for further investigations of protein-bound ammonium ions to elucidate the properties of potassium-binding sites in large proteins and also characterise the kinetic aspects of monovalent cation binding in such systems.

#### 5. Material and methods

**Sample preparations:** A sample of  $^{15}\text{NH}_4^+$  in an acidic aqueous solution was prepared by dissolving 21 mg of  $^{15}\text{NH}_4\text{Cl}$  in 2 ml of 100%  $\text{H}_2\text{O}$  containing 50 mM sodium phosphate, 2 mM EDTA, 25 mM NaCl, 2 mM  $\text{NaN}_3$ . The pH was subsequently adjusted to 2.82 to slow the chemical exchange of the ammonium protons with the  $\text{H}_2\text{O}$ . The NMR sample of the ATP binding domain of DnaK from *Thermus thermophilus* was prepared as explained previously [19]. The protein concentration was  $\sim 100 \mu\text{M}$  in 100%  $\text{H}_2\text{O}$  containing 150 mM  $^{15}\text{NH}_4\text{Cl}$ , 0.5 mM ADP, 50 mM  $(\text{NH}_4)_2\text{H}_2\text{PO}_4$ , 5 mM  $\text{MgCl}_2$ , 1 mM DTT, 1 mM  $\text{NaN}_3$  and 75 mM Tris, pH 7.5.

**NMR experiments:** The NMR experiments were performed on a Bruker Avance III 500 MHz (11.7 T) spectrometer using an HCN Prodigy probe, a Bruker Avance III 700 MHz (16.4 T) spectrometer using a TCI cryogenic inverse triple-resonance probe, and a Bruker Avance III HD 800 MHz (18.8 T) spectrometer equipped with a cryogenic inverse triple-resonance TCI probe. All spectra were measured with an external  $\text{D}_2\text{O}$  reference insert (WilmaD coaxial insert Z278513 (Sigma–Aldrich)), such that no  $\text{D}_2\text{O}$  was added to the sample buffer.

The longitudinal relaxation rates of free  $^{15}\text{N}$ -ammonium at pH 2.82 were measured at a static magnetic field of 11.7 T and 16.5 T using the pulse scheme shown in Fig. 1. For the spectra showing the initial states in Fig. 3, an inter-scan delay of 1 s was used,  $T_{\text{relax}} = 4 \text{ ms}$ , and 32 complex points were acquired in the indirect  $^{15}\text{N}$  frequency dimension. Relaxation delays  $T_{\text{relax}}$  of  $\{0.004 \text{ s}, 0.010 \text{ s}, 0.020 \text{ s}, 0.030 \text{ s}, 0.040 \text{ s}, 0.050 \text{ s}, 0.060 \text{ s}, 0.080 \text{ s}, 0.100 \text{ s}, 0.120 \text{ s}, 0.140 \text{ s}, 0.160 \text{ s}, 0.200 \text{ s}, 0.300 \text{ s}, 0.400 \text{ s}, 0.500 \text{ s}, 0.600 \text{ s}, 0.800 \text{ s}, 1.000 \text{ s}, 2.000 \text{ s}, 5.000 \text{ s}, 10.00 \text{ s}, 15.00 \text{ s}\}$  were used for all relaxation experiments. Eight scans were acquired for each FID leading to a net acquisition time of 10 h for each initial state  $\{\tau_b, \phi_4\}$ .

Longitudinal relaxation rates of  $^{15}\text{N}$ -ammonium bound to DnaK were measured at a static magnetic field strength 18.8 T. A total of 32 complex points were acquired in the indirect  $^{15}\text{N}$  frequency dimension and 32  $T_{\text{relax}}$  relaxation delays were used:  $\{0.002 \text{ s}, 0.004 \text{ s}, 0.004 \text{ s}, 0.008 \text{ s}, 0.016 \text{ s}, 0.032 \text{ s}, 0.048 \text{ s}, 0.064 \text{ s}, 0.080 \text{ s}, 0.096 \text{ s}, 0.128 \text{ s}, 0.128 \text{ s}, 0.160 \text{ s}, 0.192 \text{ s}, 0.224 \text{ s}, 0.256 \text{ s}, 0.288 \text{ s}, 0.320 \text{ s}, 0.352 \text{ s}, 0.384 \text{ s}, 0.416 \text{ s}, 0.448 \text{ s}, 0.480 \text{ s}, 0.512 \text{ s}, 0.512 \text{ s}, 0.600 \text{ s}, 0.700 \text{ s}, 0.800 \text{ s}, 0.900 \text{ s}, 1.000 \text{ s}, 1.250 \text{ s}, 1.500 \text{ s}\}$  for each initial state  $\{\tau_b, \phi_4\}$ . An inter-scan delay of 1 s was used and 40 scans were obtained for each FID, leading to total acquisition time of 34 h for each initial state.

**Data analysis:** All spectra were processed using nmrPipe [33] and signal intensities were quantified using the program FuDA [34] by assuming a common line shape for a given cross-peak during a relaxation series as described previously [15].

Relaxation decay curves for the four lines,  $I_{\alpha\alpha\alpha\alpha}(T_{\text{relax}})$ ,  $I_{\alpha\alpha\alpha\beta}(T_{\text{relax}})$ ,  $I_{\alpha\beta\beta\beta}(T_{\text{relax}})$ , and  $I_{\beta\beta\beta\beta}(T_{\text{relax}})$  as a function of  $T_{\text{relax}}$  were analysed using the propagation of the full Liouvillian and the best-fit model parameters were obtained by minimisation of the target function:

$$\chi^2(\tau_C, R_1(H_z), \mathbf{v}_0) = \sum_{\lambda=\{\alpha\alpha\alpha\alpha, \alpha\alpha\alpha\beta, \alpha\beta\beta\beta, \beta\beta\beta\beta\}} \sum_{T_{\text{relax}}} (I_{\lambda}^{\text{calc}}(T_{\text{relax}}) - I_{\lambda}^{\text{exp}}(T_{\text{relax}}))^2 / \sigma_{\text{exp}}^2 \quad (6)$$

where  $\mathbf{v}_0$  is the initial state described in the main text. The first sum is over the four lines,  $\alpha\alpha\alpha\alpha$ ,  $\alpha\alpha\alpha\beta$ ,  $\alpha\beta\beta\beta$ , and  $\beta\beta\beta\beta$ , and the second

sum is over the different relaxation delays  $T_{relax}$ . Moreover,  $I_{\lambda}^{exp}(T_{relax})$  and  $\sigma_{exp}$  are experimental intensities of the four lines observed in  $^{15}\text{N}$ - $^1\text{H}$  correlation spectra and their uncertainties, respectively,  $I_{\lambda}^{calc}(T_{relax})$  are calculated intensities obtained by numerical propagation of the initial state using the Liouvillian,  $\Gamma$ .

Calculated intensities,  $I_{\lambda}^{calc}(T_{relax})$  were obtained by first calculating a vector  $\mathbf{v}(T_{relax})$ , which describes the time-dependence of the population of the longitudinal coherences,  $\{I(N_z), \dots, I(16N_z\mathbf{H}_z\mathbf{H}_z\mathbf{H}_z\mathbf{H}_z)\}$ :

$$\mathbf{v}(T_{relax}) = \exp(-\Gamma(\tau_c, R_1(\mathbf{H}_z))T_{relax})\mathbf{v}_0 \quad (7)$$

Subsequently, the intensities of the four lines observed in the  $^{15}\text{N}$ - $^1\text{H}$  correlation spectra were calculated as described previously [20]:

$$\begin{pmatrix} I_{\alpha\alpha\alpha\alpha} \\ I_{\alpha\alpha\beta\beta} \\ I_{\alpha\beta\beta\beta} \\ I_{\beta\beta\beta\beta} \end{pmatrix} = \begin{pmatrix} -1/4 & 1 & -3/2 & 1 & -1/4 \\ -1/2 & 1 & 0 & -1 & 1/2 \\ 1/2 & 1 & 0 & -1 & -1/2 \\ 1/4 & 1 & 3/2 & 1 & 1/4 \end{pmatrix} \begin{pmatrix} I(N_z) \\ I(2N_z\mathbf{H}_z) \\ I(4N_z\mathbf{H}_z\mathbf{H}_z) \\ I(8N_z\mathbf{H}_z\mathbf{H}_z\mathbf{H}_z) \\ I(16N_z\mathbf{H}_z\mathbf{H}_z\mathbf{H}_z\mathbf{H}_z) \end{pmatrix} \quad (8)$$

Finally best-fit model parameters were determined by minimising the target function  $\chi^2$  in Eq. (6) using in-house written software based on the LMFIT python library [35].

## Acknowledgments

Dr Jochen Reinstein (MPI Heidelberg) is acknowledged for many helpful discussions and for providing purified DnaK-ABD and Dr Nicolas D. Werbeck (Bayer Pharma AG) is acknowledged for helpful discussions. Dr Christopher Waudby is acknowledged for critical reading of the manuscript and Dr Angelo Figueiredo is acknowledged for help with recording NMR spectra. The Wellcome Trust (101569/z/13/z) and the Engineering and Physical Sciences Research Council (EPSRC) are acknowledged for supporting the ISMB NMR facility at UCL and the MRC/Francis Crick Biomedical NMR centre is acknowledged for access to high-field NMR spectrometers. This research was supported by the Biotechnology and Biological Sciences Research Council (BBSRC).

## References

- [1] J.P. Grason, J.S. Gresham, G.H. Lorimer, Setting the chaperonin timer: a two-stroke, two-speed, protein machine, *Proc. Natl. Acad. Sci.* 105 (2008) 17339–17344.
- [2] S.M. Wilbanks, D.B. McKay, How potassium affects the activity of the molecular chaperone Hsc70, *J. Biol. Chem.* 270 (1995) 2251–2257.
- [3] S.L. Gantt, C.G. Joseph, C.A. Fierke, Activation and inhibition of histone deacetylase 8 by monovalent cations, *J. Biol. Chem.* 285 (2010) 6036–6043.
- [4] J.W. Riehl, K. Koch, NMR relaxation of adsorbed gases: methane on graphite, *J. Chem. Phys.* 57 (1972) 2199.
- [5] C.L. Perrin, R.K. Gipe, Rotation, solvation, and hydrogen bonding of aqueous ammonium ion, *J. Am. Chem. Soc.* 108 (1986) 1088–1089.
- [6] C.L. Perrin, R.K. Gipe, Rotation and solvation of ammonium ion, *Science* 238 (1987) 1393–1394.
- [7] Y. Masuda, Solvent effect on rotational relaxation time of ammonium ion, *J. Phys. Chem. A* 105 (2001) 2989–2996.
- [8] S.-R. Tzeng, C.G. Kalodimos, Dynamic activation of an allosteric regulatory protein, *Nature* 462 (2009) 368–372.
- [9] D. Sheppard, R. Sprangers, V. Tugarinov, Experimental approaches for NMR studies of side-chain dynamics in high-molecular-weight proteins, *Prog. Nucl. Magn. Reson. Spectrosc.* 56 (2010) 1–45.

- [10] R. Sprangers, L.E. Kay, Quantitative dynamics and binding studies of the 20S proteasome by NMR, *Nature* 445 (2007) 618–622.
- [11] S.-T.D. Hsu, L.D. Cabrita, P. Fucini, J. Christodoulou, C.M. Dobson, Probing side-chain dynamics of a ribosome-bound nascent chain using methyl NMR spectroscopy, *J. Am. Chem. Soc.* 131 (2009) 8366–8367.
- [12] A.G. Palmer, C.D. Kroenke, J.P. Loria, Nuclear magnetic resonance methods for quantifying microsecond-to-millisecond motions in biological macromolecules, *Meth. Enzym.* 339 (2001) 204–238.
- [13] C.D. Kroenke, J.P. Loria, L.K. Lee, M. Rance, A.G. Palmer, Longitudinal and transverse H-1-N-15 dipolar N-15 chemical shift anisotropy relaxation interference: unambiguous determination of rotational diffusion tensors and chemical exchange effects in biological macromolecules, *J. Am. Chem. Soc.* 120 (1998) 7905–7915.
- [14] V. Tugarinov, R. Sprangers, L.E. Kay, Probing side-chain dynamics in the proteasome by relaxation violated coherence transfer NMR spectroscopy, *J. Am. Chem. Soc.* 129 (2007) 1743–1750.
- [15] D.F. Hansen, D. Yang, H. Feng, Z. Zhou, S. Wiesner, Y. Bai, et al., An exchange-free measure of 15N transverse relaxation: an NMR spectroscopy application to the study of a folding intermediate with pervasive chemical exchange, *J. Am. Chem. Soc.* 129 (2007) 11468–11479.
- [16] D.F. Hansen, H. Feng, Z. Zhou, Y. Bai, L.E. Kay, Selective characterization of microsecond motions in proteins by NMR relaxation, *J. Am. Chem. Soc.* 131 (2009) 16257–16265.
- [17] N.V. Hud, P. Schultze, J. Feigon, Ammonium ion as an NMR probe for monovalent cation coordination sites of DNA quadruplexes, *J. Am. Chem. Soc.* 120 (1998) 6403–6404.
- [18] N.V. Hud, P. Schultze, V. Sklenár, J. Feigon, Binding sites and dynamics of ammonium ions in a telomere repeat DNA quadruplex, *J. Mol. Biol.* 285 (1999) 233–243.
- [19] N.D. Werbeck, J. Kirkpatrick, J. Reinstein, D.F. Hansen, Using  $^{15}\text{N}$ -ammonium to characterise and map potassium binding sites in proteins by NMR spectroscopy, *ChemBioChem* 15 (2014) 543–548.
- [20] N.D. Werbeck, D.F. Hansen, Heteronuclear transverse and longitudinal relaxation in AX4 spin systems: application to  $^{15}\text{N}$  relaxations in  $^{15}\text{NH}_4^+$ , *J. Magn. Reson.* 246 (2014) 136–148.
- [21] Y. Lin, A.H. West, P.F. Cook, Potassium is an activator of homoisocitrate dehydrogenase from *Saccharomyces cerevisiae*, *Biochemistry* 47 (2008) 10809–10815.
- [22] M.C. O'Brien, D.B. McKay, How potassium affects the activity of the molecular chaperone Hsc70. I. Potassium is required for optimal ATPase activity, *J. Biol. Chem.* 270 (1995) 2247–2250.
- [23] L.G. Werbelow, D.M. Grant, Intramolecular dipolar relaxation in multispin systems, *Adv. Magn. Reson.* 9 (1977) 189–299.
- [24] A. Abragam, Principles of Nuclear Magnetism, Clarendon Press, Oxford, 1961.
- [25] A.G. Redfield, in: J.S. Waugh (Ed.), *Adv. Magn. Reson.*, 1st ed., Academic Press, San Diego, 1965, pp. 1–32.
- [26] O.W. Sørensen, G.W. Eich, M.H. Levitt, G. Bodenhausen, R.R. Ernst, Product operator-formalism for the description of NMR pulse experiments, *Prog. Nucl. Magn. Reson. Spectrosc.* 16 (1983) 163–192.
- [27] D.F. Hansen, J.J. Led, Implications of using approximate Bloch-McConnell equations in NMR analyses of chemically exchanging systems: application to the electron self-exchange of plastocyanin, *J. Magn. Reson.* 163 (2003) 215–227.
- [28] A.J. Shaka, J. Keeler, T. Frenkiel, R. Freeman, An improved sequence for broadband decoupling – Waltz-16, *J. Magn. Reson.* 52 (1983) 335–338.
- [29] D.F. Hansen, P. Vallurupalli, L.E. Kay, Measurement of methyl group motional parameters of invisible, excited protein states by NMR spectroscopy, *J. Am. Chem. Soc.* 131 (2009) 12745–12754.
- [30] N.R. Skrynnikov, O. Millet, L.E. Kay, Deuterium spin probes of side-chain dynamics in proteins. 2. Spectral density mapping and identification of nanosecond time-scale side-chain motions, *J. Am. Chem. Soc.* 124 (2002) 6449–6460.
- [31] Y. Xue, M.S. Pavlova, Y.E. Ryabov, B. Reif, N.R. Skrynnikov, Methyl rotation barriers in proteins from  $^2\text{H}$  relaxation data. Implications for protein structure, *J. Am. Chem. Soc.* 129 (2007) 6827–6838.
- [32] A. Esadze, D.-W. Li, T. Wang, R. Brüschweiler, J. Iwahara, Dynamics of lysine side-chain amino groups in a protein studied by heteronuclear  $^1\text{H}$ - $^{15}\text{N}$  NMR Spectroscopy, *J. Am. Chem. Soc.* 133 (2011) 909–919.
- [33] F. Delaglio, S. Grzesiek, G.W. Vuister, G. Zhu, J. Pfeifer, A. Bax, Nmrpipe – a multidimensional spectral processing system based on Unix pipes, *J. Biomol. NMR* 6 (1995) 277–293.
- [34] S.M. Kristensen, D.F. Hansen, FuDA: A function and data fitting and analysis package. (smk@kiku.dk), (2006).
- [35] M. Newville, T. Stensitzki, D.B. Allan, A. Ingargiola, J.J. Helmus, E.O. Le Bigot, et al., LMFIT (2014).